A High-Gain Nested Patch Antenna with Strong Coupling and Parasitic Elements for Dual-Band Wireless Local Area Network Applications

Yavuz ASCI [a,*], Kaan Bakircioglu [b], Mustafa Secmen [c].

a. Department of Electrical and Electronics Engineering, Usak University, 64300, Usak, Turkey
b. Graduate School, Yasar University, 35100, Izmir, Turkey
c. Department of Electrical and Electronics Engineering, Yasar University, 35100, Izmir, Turkey

* Corresponding author: yavuz.asci@usak.edu.tr (Yavuz Asci)

Keywords

dual-band antenna;
high-gain;
low profile;
strong-coupled nested patches;
single feed;
wireless local area network (WLAN).

Abstract

This study presents a high-gain, single-feed, wideband, and dual-band antenna covering the complete 2.4 GHz and 5.2 GHz Wireless Local Area Network (WLAN) frequency spectra. The proposed design features two nested radiators: an inner E-shaped patch operating at the higher (5.2 GHz) band and an outer rectangular patch for the lower (2.4 GHz) band. These radiators are tightly coupled to enhance the bandwidth at 5.2 GHz, while parasitic elements are integrated into the outer radiator to ensure full coverage of the 2.4 GHz band. A single-feed mechanism is employed to simplify the feeding structure and fabrication, thereby reducing overall costs. A grounded pin is utilized for band isolation, whereas the strong coupling between the inner and outer patches enables precise control and expansion of the operational bandwidths. The prototype was fabricated and measured, demonstrating -10 dB impedance bandwidths of 2.39–2.51 GHz and 4.95–5.82 GHz for the lower and higher bands, respectively. The antenna maintains a low profile with dimensions of 77 mm × 75 mm × 6.5 mm and achieves measured peak gain values of 7.8 dBi and 7.5 dBi for the lower and higher bands, respectively. Furthermore, the radiation patterns exhibit stable directional characteristics, indicating high isolation between the bands. The experimental results confirm that the proposed antenna fully spans 2.4 GHz and 5.2 GHz spectra, meeting key design objectives: wideband operation, compact size, high gain, and stable radiation performance. These distinct advantages make antenna a suitable candidate for next-generation WLAN routers, MIMO access points, and high-efficiency WLAN transceivers.

1. Introduction

Wireless Local Area Network (WLAN) standards are determined by the needs of the scenario, such as the maximum transmit/receive range and power consumption. The rising demand for higher data transmission rates has sparked a dramatic increase in WLAN technology, pushing service providers to search for terminals that operate on dual or multiple frequency band. Consequently, there is a growing demand for multifunctional antennas that not only have dual/wide operating band characteristics but also high gain and low profile, while ensuring ease of fabrication and smooth integration with other RF devices, currently used in a variety of applications.

Although low-profile patch antennas are increasingly favoured for modern wireless systems due to their versatility, the ongoing trend toward device miniaturization presents significant design challenges. While printed antennas are excellent candidates for size-constrained applications, they are subject to three fundamental trade-offs: inherently narrow bandwidth, a gain characteristic typically proportional to physical dimensions, and low efficiency resulting from increased dielectric losses, particularly at high frequencies [1, 2].

Although various methods have been explored to broaden the bandwidth of printed antennas, conventional approaches typically involve increasing bandwidth is generally either to increase the substrate thickness which lowers the quality factor (Q) results in wideband impedance matching or to use high dielectric material as a substrate [3–9]. In [3], parasitic structures are integrated into the radiating layer to enhance the impedance bandwidth; however, this approach inevitably expands the antenna's footprint. In [4], an elliptical radiator is introduced to replace the circular radiator to enhance wideband performance.

Alternatively, incorporating slots into the antenna geometry has emerged as an effective strategy. This method can excite additional resonant modes to widen the bandwidth without altering the physical footprint or thickness, though it requires careful optimization as it may exert either a constructive or destructive influence on both bandwidth and gain. In [5], adding a semi-circular slot to the top edge of the rectangular main radiator and a rectangular slot to the middle of the radiator structure results in wideband characteristics. In [6], utilizing E-shaped slots with coupled branches and shorting pins, wideband performance is realized. In [7], double L-shaped slits is employed for wideband operation. In [8], the wideband characteristic is derived by integrating the U-slot into the rectangular patch antenna. An ultrawideband (UWB) coplanar waveguide-fed (CPWF) textile antenna for wearable electronics is presented in [9], where circular and I-shaped slots are employed to broaden the impedance bandwidth.

Many studies and methods have been conducted to convert the wideband antennas into dual or multi-band antennas. Adding notches at undesired bands in the frequency response of the wideband antenna is frequently used to separate and isolate the desired bands and to obtain multi-band. Adding slots, slits or stubs is important because they can be easily implemented and control the surface currents without increasing the antenna's footprint. Modifying the dimensions and locations of the slots/slits/stubs increases the current path and introduces nulls at undesirable operating frequencies. This improves the isolation between the two operating bands. This is particularly crucial when the operating frequencies are very close to each other. In [10], single feed (coaxial) wideband "U"-shaped slot patch antenna is converted to a dual-band antenna by adding second "U"-shaped slot that adds notch to the wideband antenna. In [11], by using "hook"-shaped slits in the trapezoid patch (radiator) and inverted Ω-shaped slots in the feed line that adds two notched bands, an ultrawideband antenna is converted triple-band antenna. In [12], the symmetrical "F" and "U" slots are incorporated into the rectangular patch to achieve multiband antenna.

Numerous multiband antennas based on printed monopole, dipole and patch have been proposed [13–19]. In [13], a planar multi-band antenna for WiMAX and WLAN bands is studied. The use of four strips with different lengths as radiating elements allows multiband characteristics to be achieved. In [14], a compact planar monopole antenna is investigated for operation at four ISM bands: 2.4 GHz, 915 MHz, 866 MHz and 433 MHz, where the meander line approach is used to achieve compactness. In [15], an omnidirectional sleeve dipole antenna operating at 2.4 GHz, 5 GHz, and 6 GHz frequencies is presented. The multi-band functionality in [16] is obtained by incorporating two inverted "L"-shaped slots into the radiator of the monopole antenna. Although these mentioned antennas exhibit compact dimensions, the gains of the printed monopole/dipole antennas are generally limited and difficult to increase to high levels. In [17], a miniaturized multiband antenna that spans all WiMAX and WLAN bands is presented. The miniaturization is accomplished by adding "Y"-shape radiator into the circular main radiator and employing a triangular shaped defected ground structure (DGS). In [18], the quadruple band is formed using two stacked microstrip antennas, which are excited by an "L"-shaped feed line. In [19], a triband multi-input multi-output (MIMO) planar antenna with DGS is outlined. Thin microstrip lines are used between antennas to increase isolation. However, all these antennas are generally compact but suffer from low-gain at the given bands due to their multiband operation.

Several approaches are outlined in the literature about dual-band antennas [20–29]. A fork shaped monopole patch antenna with a chip inductor [20], an inverted-F antenna with a "U"-shaped slot [21], a triangular-shaped printed antenna with a grounded pin [22], and a split-ring monopole antenna [23] are investigated.

Other approaches have also been studied, such as two nested split-ring radiators [24], a monopole antenna with two strips one of which is a rectangular slit in the asymmetric ground plane and the other is a rectangular projection strip serving as a radiator [25], an equilateral triangular microstrip patch loaded with slots near the side and bottom edges [26], and a single-feed two-layer antenna with "E"-shaped slot in the lower-layer patch and "U"-shaped slot in the top-layer patch [27].

In [28], single feed, single layer dual-band antenna with two "U"-shaped slots is studied. The higher bandwidth of the proposed antenna is improved by using one of the "U"-shaped slots. The second "U"-shaped slot, which is inverted relative to the first, is added to eliminate the asymmetric current distribution that causes distortion of the dual-beams. In [29], a dual-band stacked antenna is reported, where two circular patch microstrip structures are used to obtain dual-band characteristics. An annular ring, coupled to the upper circular patch, and grounded vias, is used to broaden the bandwidth of the antenna.

Since local WLAN frequency allocations vary globally, developing a single antenna capable of covering the full 2.4 – 2.484 GHz (IEEE 802.11b/g) and 5.15 – 5.825 GHz (IEEE 802.11a) bands is essential for ensuring universal connectivity. Nevertheless, simultaneously achieving high gain, dual-band functionality, and robust radiation characteristics within a compact footprint remains a formidable design challenge. While extensive research has been conducted to address these trade-offs, as documented in the preceding literature, the demand for more efficient and integrated solutions continues to drive the search for optimized antenna architectures.

In this paper, the antenna's cost and profile are minimized by utilizing a single patch and feed configuration, which eliminates the necessity of a balun structure typically required to mitigate asymmetric current distributions in printed dipoles. To achieve a compact footprint, the outer and inner patches are positioned in close proximity. However, this spatial constraint introduces design complexities, as strong mutual coupling between the patches significantly influences the overall antenna characteristics. Specifically, the dimensions of one patch inherently affect the performance of the other; for instance, modifying the outer patch dimensions not only shifts the lower resonant frequency but also potentially deteriorates the impedance matching at the upper band. To address this interdependence, a simultaneous optimization of both inner and outer patch dimensions is conducted to identify the ideal parameters that satisfy the dual-band requirements.

Consequently, this study presents a novel, compact, and high-gain dual-band microstrip antenna tailored for the 2.4 GHz and 5.2 GHz worldwide WLAN bands. The proposed design successfully maintains a minimal physical volume while simultaneously enhancing gain and bandwidth performance.

The remainder of this study is organized into four sections. Section 2 details the design method and antenna structure where the design and simulations are conducted in CST Design Studio. The effect of key structure parameters on antenna characteristics is employed with the help of parametric studies. A comparison of the simulation and measured results for the proposed dual-band antenna about return loss, gain and radiation patterns for lower and upper frequency bands is provided in Section 3. Section 4 concludes the study with a summary of findings.

2. Proposed single-feed, dual-band antenna structure and analysis

2.1. Dual-band antenna structure and design

Figure 1 depicts the geometry of the proposed high-gain, dual-band, low-profile, single-feed antenna, along with its structural parameters. The proposed dual-band antenna is made up of three main parts, comprising radiating patches, a pin section consisting of an excitation pin and a grounded pin, and a ground plane. The radiating section comprises two nested rectangular radiator patches connected by a microstrip line. While the outer patch with the parasitic lines at the left and right edges is for the 2.4 GHz band, the inner patch is for the 5.2 GHz band.

Using a thicker substrate and a material with a low relative permittivity (ε_r) are both effective methods of enhancing the impedance bandwidth of a patch antenna. A lower ε_r reduces the antenna's quality factor (Q), resulting in a wider impedance bandwidth. Similarly, a thicker substrate allows for a greater fringing field, which contributes to a wider bandwidth. For this purpose, a thick air substrate with a height of *h1* as shown in Figure 1 is used. To ensure mechanical stability of the copper radiating parts during manufacturing of the antenna and increase the total thickness of the structure, the patches and lines are printed on a one-sided Rogers 4003C substrate with ε_r = 3.55 and height of 1.52 mm, which is placed above the air substrate. However, while thicker and lower ε_r substrates can improve bandwidth, they must be carefully implemented in probe-fed designs due to their impact on impedance matching and antenna size. As the substrate becomes thicker, achieving proper impedance matching becomes more difficult due to the increased inductive nature of the probe feed, which can lead to higher return loss and consequently reduce wideband performance. Moreover, increasing the substrate thickness also increases the physical size of the antenna (height and length) for a given resonant frequency. This is because the effective dielectric constant decreases with lower ε_r and thicker substrates, which in turn increases the guided wavelength. Furthermore, as the height of the substrate increases and becomes comparable to the wavelength (exceeding $\lambda_0/10$), the gain along broadside direction dramatically decreases, as predicted by the image theory for microstrip patch antennas. For instance, a null occurs along the broadside direction, theoretically when the substrate height reaches $\lambda_0/4$. Therefore, an optimum height for substrate and probe feed of the antenna is needed to provide sufficiently wide bands at dual applications of WLAN. Considering the highest operating frequency of 5.8 GHz ($\lambda_0 \approx$ 52 mm), the air substrate height is selected to be less than $\lambda_0/10$, corresponding to a thickness of 5 mm.

Since the total height of the structure is primarily composed of an air substrate, the guided wavelength closely approximates the free-space wavelength. Consequently, the initial dimensions of both the inner and outer rectangular patches are chosen to be approximately one-quarter of the free-space wavelength ($\lambda_0/4$) at their respective center frequencies since they are shorted-pin patches at the one edge. These patches are printed on the upper side of the RO4003C substrate to facilitate the probe-fed configuration.

The inner rectangular patch is supported by optimised slots and slits arranged symmetrically relative to the feed, is used to improve the antenna's bandwidth/gain. The dimensions of each radiating element are optimised for the desired resonant frequencies of the 2.4 GHz (lower) and 5.2 GHz (higher) operating frequency spectrums. The second part is the probe feeding and grounded (shorted) pin. While the grounded pin is used to isolate two bands, the inner feed conductor of SMA connector extended through the heights of air and Rogers substrates provide excitation for the inner patch on the top layer. An impedance tuning is possible with the optimized location of this feed on the patch, and Teflon material (PTFE) around feed conductor helps for wideband matching. As the final part of the proposed dual-band antenna the lateral dimensions of the ground plane, which is located below and separated from the patch layer by air and Rogers substrates, are chosen the same as those of both substrates. To keep the lateral dimensions of the antenna as compact and to obtain the gain values as reasonably high, the length and width of the ground plane is L = 75 mm by W = 77 mm, respectively, which almost corresponds to $0.6\lambda_0$ at the lower band and more than one wavelength at the upper band. The single SMA connector [30] is used to the structural integrity of the patch and the ground plane.

Due to the single-feed configuration, proper isolation between the 2.4 GHz (the lower) and 5.2 GHz (the upper) frequency bands is essential. To effectively separate the lower (2.4 GHz and upper (5.2 GHz) frequency bands, a grounded pin is inserted into the microstrip line connecting the inner and outer patches. It generally plays a critical role in preventing surface currents from coupling between the two patches [31, 32], thereby isolating the operating bands and enhancing the -10 dB impedance bandwidth. This grounded pin in Figure 1 actually isolates the regions above and below the grounded pin by particularly suppressing the coupling of the 5.2 GHz band below grounded pin such that it is quite difficult to control and arrange the 5.2 GHz band without the given grounded pin. On the other hand, since the feed SMA is located on the inner patch, the isolation of fields/currents of 2.4 GHz is limited. Even, the performance of the lower frequency band could be potentially boosted and length of the outer patch could be shortened if the upper edge of the inner patch was physically connected to upper strip of the outer patch. However, this makes the control of the 5.2 GHz band quite complicated since the currents of this band will also flow on the outer patch, effectively.

As the solution of the issues described in the preceding paragraph and one of the key novelties of the antenna, a strong coupling between the upper strip of the outer patch and the upper edge of the inner patch, which is mainly optimized by the parameter of *y4* in Figure 1, is enabled to simultaneously control of both the 2.4 GHz and 5.2 GHz bands. This coupling causes the upper strip to act as an extension of the inner patch, modifying the resonance at 5.2 GHz, while also creating an effective current path between the upper strip and the feed, which impacts the outer patch and the 2.4 GHz band. As to be explained in Section 2, this coupling is also responsible from the changes in the resonances of both bands due to width-related parameters such as *x1* and *x12* being other parameters to arrange the coupling level. Since the coupling influences effective length of both bands and patches, the antenna without the coupling likely requires larger overall lengths and dimensions to achieve resonances. Therefore, the coupling effects also utilize a certain reduction in the overall length of the antenna and improved/increased compactness.

The outer patch alone is insufficient to fully cover the lower frequency band. To address this, parasitic edges having almost the same length with outer patch are added. Although these strips slightly increase the overall footprint of the antenna, they extend the effective current path, which ensures full coverage of the lower band. The role of these parasitic edges is crucial such that they improve bandwidth and radiation characteristics without requiring additional feeding structures. The SMA feed is located at a position of maximum electric field intensity, ensuring optimal excitation of the radiating structure. This location is further refined through parametric optimization to achieve improved impedance matching and gain over both bands. The feed pin and the grounded pin have radii of 0.64 mm and 0.5 mm, respectively, and are selected from standard commercially available components. The grounded pin is electrically connected to the common ground shared by both the SMA connector and the ground plane. The CST Design Studio with frequency domain solver is used for the design and to obtain resonance at the intended operating frequency bands of the proposed antenna. The ultimate dimensions of the proposed dual-band antenna are tabulated in Table 1 where the effects of most of these parameters are investigated in Section 2.

To gain a better insight of the dual-band and radiation characteristics, the simulated results of the surface current distributions at 2.4 and 5.2 GHz are illustrated in Figure 2(a) and 2(b), respectively.

At lower frequency (2.45 GHz), as expected, the surface currents are mainly distributed on the outer radiating patch. which has a length of *y2* = 35 mm, being close to corresponding to a quarter-wavelength at this frequency $\lambda_0/4 \approx 31.25$ mm. The influence of the grounded pin is clearly observed at this frequency, as it enhances isolation between the two operating bands by suppressing undesired coupling.
At the higher frequency band (5.4 GHz), the surface currents are predominantly localized on the inner patch, which has a length of *y4* = 17 mm that is again almost exactly one quarter of the wavelength at 5.4 GHz, which indicates the resonance at the 5.4 GHz band. These current distributions confirm the dual-resonant nature of the antenna. Figure 2(a) also reveals some current presence on the inner patch at 2.45 GHz, which is attributed to the proximity of the feed point (SMA connector). Nevertheless, the dominant contributors at this frequency are the outer and parasitic patches, collectively supporting the lower-band resonance. Similarly, at 5.4 GHz, strong surface currents on the inner patch confirm its role in supporting the higher-band resonance. The simulation results also indicate that removing the grounded pin leads to destructive interference between surface currents on the inner and outer patches. This results in a noticeable degradation in both impedance bandwidth and radiation gain.

2.2. Parametric studies of the proposed dual-band antenna

Parametric studies are performed in CST to provide a better understanding of the working mechanism and to achieve the design goals, fully covering the WLAN 2.4 GHz and 5.2 GHz bands with high-gain while maintaining the compactness of the proposed dual-band antenna. This analysis encompasses nearly all antenna dimensions. The most dominant and sensitive parameters influencing impedance matching, resonance frequency shifts, peak gain, and bandwidth are chosen. Moreover, a suitable step size and sweep range are selected to clearly illustrate the influence of these parameters on the overall antenna performance.
During the parametric scanning routine, only one parameter was varied at a time while keeping the others were held constant. Although there are several parameters as given in Table 1, this section only focuses on the most critical ones, which can be divided into 3 sub-sections: the parameters affecting mainly only the 2.4 GHz band, only the 5.2 GHz band, and both bands.

2.2.1. The parameters affecting mainly the 2.4 GHz band

As described in Section 1, while the parameters of the outer patch and parasitic element mainly change the resonance frequency around 2.45 GHz, the inner patch parameters affect the upper band. By considering Figure 1, the parameters above the feed line/transition with the width of *x8* (transition width) can be stated to be responsible for the upper band. This explanation is supported by the results given in Figure 3 where the parameters of *y2* (the outer patch length), *x8* and *y10* (the position of grounded pin below transition) mainly have a considerable effect to resonance frequency and bandwidth of lower band; however, their contributions to the upper band are negligible.
The results for the ultimate dimensions of the antenna, as given in Table 1, are presented as the first parameter value in each subfigure of Figure 3. (and also, on Figure 4 and Figure 5 in the proceeding subsections). Based on these simulation results, the designed antenna attains a 10 dB impedance bandwidth for 2.39–2.48 GHz and 5.0–5.87 GHz, which fully covers both WLAN bands of 2.4 and 5.2 GHz. Besides, the proposed dual-band antenna has more than 6.6 dBi and 6.1 dBi broadside gain over the 2.4 and 5.2 GHz bands, respectively. The peak gains are 7.8 and 7.5 dBi on the aforementioned bands. Considering that the antenna's overall dimensions are approximately half a wavelength at the lower frequency and one wavelength at the higher frequency band, these values can be considered as high-gain. The optimization process also aims to maximize the possible gain values over the given bands. For instance, when Figure 3(d) is examined, the gain values over the 2.4 GHz band and especially at 2.4 GHz are observed to be sensitive to the parameter value of *y2*, which has also slight effect on the 5.2 GHz as to be explained in the following subsection.

2.2.2. The parameters affecting mainly the 5.2 GHz band

The input reflection coefficient and gain variations as a function of the parameters mainly changing and optimizing the 5.2 GHz band are given in Figure 4.
The changes as a function of the coaxial feed position are depicted in Figure 4(a) and 4(d). The feed position has a substantial effect on the 5.2 GHz band whereas it has only a slight effect on the 2.4 GHz band, which is an expected result since the excitation pin is placed on the inner patch. Shifting the feed position longitudinally towards the grounded pin direction (by increasing the *y7* value) shifts the resonance to lower frequencies and decreases boresight gain of the antenna at the upper frequency band. Similarly, the parameter *y6*, which is another longitudinal dimension of the inner patch antenna, is quite influential on the upper frequency band as plotted in Figure 4(b) and 4(e).
One interesting parameter that mainly affects the 5.2 GHz band, but not the 2.4 GHz band is *x1* (outer patch width). Although the parameter seems to be the part of outer patch, it notably affects the inner patch's resonance frequency and response rather than those of the outer patch. Since *x1* is the width of the outer patch and it is well-known that the resonance frequency is not affected the patch width of the antenna.

As indicated in Figure 4(c), it is reasonable to say that there has been almost no change in the response of the 2.4 GHz band. On the other hand, considering Figure 1, there is a strong coupling between the upper edge of the inner patch and the horizontal strip part of the outer patch beyond this upper edge. This strip part behaves as an extension for the effective resonance length of the inner patch due to strong coupling and is controlled with the dimensions of *x1* and *y2*. Therefore, varying the width of this strip modifies the resonance frequency and response of the upper band in the 5.2 GHz range.

2.2.3. The parameters affecting both bands

The input reflection coefficient and gain variations as a function of the parameters, which influence and optimize both bands are given in Figure 5.

In Figure 1, the insets of the inner patch with the length of y8 (stub length) are critical for the response and characteristics of the antenna where they behave as matching stubs for both 2.4 and 5.2 GHz band. Their lengths and relative horizontal positions in the inner patch along with the width of the inner patch, x12, are important for proper tuning of the resonance at 2.4 and 5.2 GHz bands. Therefore, as illustrated in Figure 5, the parameters related to these stubs (y8 and x12) significantly change the responses of both bands.

As the last parameter considered in Figure 5, the dimension of y4 (inner patch length) is expected to influence the resonance in the upper 5.2 GHz band. On the other hand, this parameter is also crucial for arranging the coupling level between the inner patch and the upper strip of the outer patch. The value of y4 = 15 mm in Figures 5(c) and 5(f) can be considered to represent a case of almost 'no coupling', which produces inadequate results in both bands. As y4 increases, the coupling level becomes stronger and the performance especially at 2.4 GHz is substantially improved by shifting the resonance frequency towards right. However, the parameter has an optimum value of y4 = 17 mm that the 10 dB impedance bandwidth and gain values begin to reduce at the 5.2 GHz band for the higher value of this parameter where the case of y4 = 17.5 mm (not given in Figure 5) is the case connecting metals of the inner patch and the upper strip of the outer patch, physically.

2.3. Impedance Bandwidth Enhancement via Parasitic Strips

In order to investigate the impact of the parasitic strips and to present how these parasitic strips (lines) specifically interact with the outer patch current path to achieve this widening effect at 2.4 GHz band, the simulations are performed with and without these elements. Figure 6(a) indicates that the inclusion of parasitic patches enhances the lower impedance bandwidth, thereby achieving full coverage of the lower WLAN frequency band. The structure without parasitic elements has only one resonance frequency at about 2.43 GHz; therefore, has narrower bandwidth, which does not satisfy overall 2.4 GHz WLAN band. However, the incorporation of parasitic elements into outer patch antenna introduces additional resonant paths that are electromagnetically coupled to the antenna. These strips placed in close proximity to the outer patch generate an additional resonance at about 2.48 GHz as shown in Figure 6(a). Therefore, the closely spaced resonant frequencies of 2.43 GHz and 2.48 GHz provide sufficient bandwidth at 2.4 GHz band for the outer patch. As illustrated in Figure 6(b), the parasitic patches exhibit negligible influence on the higher frequency band since parasitic strips have no interaction with inner patch.

3. Manufacturing of the Prototype, Results and Discussion

After the design and simulation steps given in Section 2, the proposed dual-band antenna in Figure 1 is fabricated with the optimized dimensions from Table 1 as depicted in Figure 7. The radiating element, comprising nested patches and parasitic strips, is etched on a 1.52 mm thick, a single-sided Rogers RO4003C substrate with lateral dimensions of 75 mm by 77 mm, as seen from top in Figure 7(a). By considering the skin depth values of copper at the lowest frequencies of the antenna around 2.4 GHz, a thin (on the order of few microns) copper plane without a substrate beneath can be actually sufficient for the ground plane of the antenna such that the overall structure can only contain one substrate of Rogers RO4003C as depicted in Figure 1. However, by considering manufacturing operations such as the soldering operations of shorting pin and SMA connector to ground plane and preventing the deformation of thin copper layer, a single copper-sided FR4 substrate with cladding thickness of 35 mikron is used as the common ground plane of the antenna. Therefore, this one-sided second substrate given in Figure 7(b) is only used for the purpose of providing mechanical stability of the ground plane where the substrate below the ground plane has no effect in the performance of the antenna. The air gap between RO4003C and FR4 substrates is supported with the foam spacers at the corners having the thickness of about 5 mm as given in Figure 7(b).

The fabricated antenna's reflection coefficient ($|S_{11}|$) values are measured with Anritsu MS2028C VNA as shown in Figure 8(a) and 8(b), and the gain values along with radiation patterns are obtained with the measurements in an anechoic chamber at the Yasar University Antenna and Microwave Laboratory as depicted in Figure 8(c).

The measured and simulated reflection coefficients and boresight gains are shown in Figure 9(a) and Figure 9(b), respectively, for comparison. Two impedance bandwidths for $|S_{11}| < -10$ dB are 120 MHz for the lower frequency band (2.39 – 2.51 GHz) and 870 MHz for the upper frequency band (4.95 – 5.82 GHz) of the proposed dual-band antenna, as demonstrated in Figure 8(a). Considering the measured results, the proposed antenna shows dual-band performance, fully spanning the 2.4 and 5.2 GHz bands of WLAN, showing that the impedance bandwidth goal has been achieved. Based on the 10 dB impedance bands obtained from the simulation results as 2.39 – 2.48 GHz and 5.00 – 5.87 GHz, the shift in the resonant frequencies between the measurement and simulation results is less than 1%, which can be owing to the fabrication tolerances and deviation in the material properties of the RO4003C substrate. As evident from Figure 9(b), the measured boresight gain values of the proposed dual-band antenna are greater than 6.6 dBi and 6.1 dBi for the 2.4 GHz and 5.2 GHz bands, respectively. Specifically, the measured peak gains reach 7.8 dBi at 2.4 GHz and 7.5 dBi at 5.2 GHz, demonstrating that the antenna meets the high-gain criteria. Overall, a reasonable agreement is observed between the measured and simulated gains, with maximum differences of only 0.1 dB and 0.4 dB for the 2.4 and 5.2 GHz bands, respectively.

Figure 10(a) – 10(d) depict the measured and simulated normalized radiation patterns for the frequencies of 2.45 GHz at the two principal planes, the E-plane ($\phi = 90°$, *YoZ*) and H-plane ($\phi = 0°$, *XoZ*), defined according to the coordinate axis in Figure 1. The antenna's radiation patterns are stable, demonstrating that there is no tilt in the main lobe and the peak gains are aligned with the boresight direction at both planes and operating frequency bands. Furthermore, 3 dB beamwidth values are found to be close to each other at 2.45 GHz and 5.4 GHz for each plane. The antenna exhibits almost linear polarization (θ-pol at E-plane and ϕ-pol at H-plane) such that the cross-polarization (X-pol) levels (normalized with respect to the maximum Co-pol gain) are measured lower than -15 dB within the beamwidth for both planes at 2.45 GHz and within the full angle range for both planes at 5.4 GHz. A comparison is provided in Table 2 between the proposed dual-band WLAN antenna and the state-of-the-art dual-band antennas occupying 2.4 and/or 5.2 GHz WLAN bands as outlined in the literature. The proposed antenna has the highest peak gain at the lower (2.4 GHz) band among all studies in Table 2. Moreover, for the higher 5.2 GHz band, the studies having similar peak gain values are electrically larger in size [10], [27], [29] and/or have narrower band not including the whole WLAN 5.2 GHz [28] as compared to the proposed antenna. The antenna has optimum performance in terms of the coverage of two WLAN bands, peak gain values and compact dimensions among the antennas in Table 2.

4. Conclusions

A novel, single feed, compact high-gain dual-band antenna that fully spans WLAN 2.4 GHz and 5.2 GHz bands is experimentally and numerically investigated. The dual-band performance is implemented via strongly coupled nested patches. The strong coupling between the uppermost part of the inner patch and the outer patch makes it possible to fine-tune both bands, resulting in a more compact structure. Although the antenna is fed from a single point, the 2.4 GHz and 5.2 GHz bands are decoupled from each other by using a grounded pin. The 2.4 GHz band has been widened by parasitic strips (lines), which extend the effective current path and are incorporated into the left and right sides of the outer patch. To achieve design goals such as high gain and full coverage of the WLAN 2.4 GHz and 5.2 GHz spectrum, as well as a compact structure, many parametric studies are conducted. The optimal dimensions of the structure are obtained and the antenna is fabricated accordingly. The dimensions of the proposed dual-band antenna are $0.62\lambda_c \times 0.61\lambda_c \times 0.05\lambda_c$ offering a compact size. The measured results reveals that the antenna has impedance bandwidths of 120 MHz (2.39–2.51 GHz) and 870 MHz (4.95–5.82 GHz) and with peak gains of 7.8 dBi and 7.5 dBi for the 2.4 GHz and 5.2 GHz WLAN bands, respectively. Due to its compact design, high gain, and single-feed operation without mutual interference between the two bands, the proposed antenna is ideal for worldwide WLAN applications.

Acknowledgments
This work was supported by Scientific and Technological Research Council of Turkey (TUBITAK) under Grant No 119C171. The authors thank TUBITAK for their support.

References

[1] Keshwala, U., Rawat, S., and Ray, K. "Half hexagonal shaped UWB antenna with triple band notch using resonating structures for wireless communication", *Scientia Iranica*, **31**(17), pp. 1547-1555 (2024). doi: 10.24200/sci.2023.59268.6145
[2] Iriqat, S., Yenikaya, S. and Secmen, M. "Design and characterization of a circular ring monopole antenna and its MIMO configuration for sub-6 GHz, sub-7 GHz and mm-wave 5G applications", *Phys. Scr.*, **99**(12), pp.125533, (2024). doi: 10.1088/1402-4896/ad8e97
[3] Luo, Z., Su, T. and Xu K. -D. "A single-layer low-profile dual-wideband monopolar patch antenna with shorting vias and parasitic annular sectors", *IEEE Antennas and Wireless Propagation Letters*, 22(2), pp. 432-436 (2023). doi: 10.1109/LAWP.2022.3215210
[4] Suvalka, R., Agrahari, S., Yadav, Ajay K.S., et al. "EBG and SRR loaded triple band notched UWB antenna", *Scientia Iranica*, **31**(5), pp. 458-468, (2024). doi: 10.24200/sci.2022.59023.6032
[5] Rajiv, A. and Bactavatchalame, P. "A wideband coplanar waveguide fed antenna for fifth generation internet of things applications", *Scientia Iranica*, in press (2026). doi: 10.24200/sci.2025.66839.10274
[6] Guo, L. -L., Chen, G. -T. and Wang, L. "A wideband single-layer E-shaped microstrip antenna with coupled branches", *2023 IEEE 11th Asia-Pacific Conference on Antennas and Propagation (APCAP)*, Guangzhou, China, pp. 1-2. (2023). doi: 10.1109/APCAP59480.2023.10469959
[7] Kim, Tae-Hyun and Park, Dong-Chul. "Compact dual-band antenna with double L-slits for WLAN operations", *IEEE Antennas and Wireless Propagation Letters*, **4**, pp. 249-252 (2005). doi: 10.1109/LAWP.2005.852576
[8] Lee, K. F., Luk, K. M., Tong, K. F., et al. "Experimental and simulation studies of the coaxially fed U-slot rectangular patch antenna", *IEE Proceedings - Microwaves, Antennas and Propagation*, **144**, pp. 354–358 (1997). doi: 10.1049/ip-map:19971334
[9] Sharma, M. D., Yadav, A., Singhal, S., et al. "CPW fed textile UWB antenna for IoT and wearable applications", *Scientia Iranica,* in press (2025). doi: 10.24200/sci.2025.64547.9070
[10] Mok, W. C., Wong, S. H., Luk, K. M., et al. "Single-Layer single-patch dual-band and triple-band patch antennas", *IEEE Transactions on Antennas and Propagation*, **61**(8), pp. 4341-4344 (2013). doi: 10.1109/TAP.2013.2260516
[11] Parchin, N. O., Amar, A. S. I. and Soliman, M. A. "An Ultra-Wideband trapezoid monopole antenna exhibiting dual notch bands using an inverted Ω-Shaped slot and Hook-shaped slits", *2024 International Telecommunications Conference (ITC-Egypt)*, Cairo, Egypt, pp. 753-756 (2024) doi: 10.1109/ITC-Egypt61547.2024.10620459
[12] Moosazadeh, M. and Kharkovsky, S. "Compact and small planar monopole antenna with symmetrical L- and U-shaped slots for WLAN/WiMAX applications", *IEEE Antennas and Wireless Propagation Letters*, **13**, pp. 388-391 (2014). doi: 10.1109/LAWP.2014.2306962
[13] Mehdipour, A., Sebak, A. -R., Trueman, C.W. and Denidni, T.A. "Compact multiband planar antenna for 2.4/3.5/5.2/5.8-GHz wireless applications", *IEEE Antennas and Wireless Propagation Letters*, **11**, pp. 144-147 (2012). doi:10.1109/LAWP.2012.2185915

[14] Selek, A., Turkmen, C. and Secmen, M. "Compact planar folded monopole antenna with coupling mechanism for quad ISM band, GNSS and UMTS applications", *2018 11th German Microwave Conference (GeMiC)*, Freiburg, Germany, pp. 211-214 (2018). doi: 10.23919/GEMIC.2018.8335067

[15] Yan, F. -G., Dong, X. -N., Fang, Y. -J., et al. "A multi-band sleeve dipole antenna for 2.4/5/6 GHz WLAN application", *2023 International Conference on Microwave and Millimeter Wave Technology (ICMMT)*, Qingdao, China, pp. 1-3 (2023). doi: 10.1109/ICMMT58241.2023.10277601

[16] Chen, H., Yang, X., Yin, Y.Z., et al. "Triband planar monopole antenna with compact radiator for WLAN/WiMAX applications", *IEEE Antennas and Wireless Propagation Letters*, **12**, pp. 1440-1443 (2013). doi: 10.1109/LAWP.2013.2287312

[17] Pei, J., Wang, A. -G., Gao, S. and Leng, W. "Miniaturized triple-band antenna with a defected ground plane for WLAN/WiMAX applications", *IEEE Antennas and Wireless Propagation Letters*, **10**, pp. 298-301 (2011). doi: 10.1109/LAWP.2011.2140090

[18] Fujimoto, T. and Yoshitake, Y. "Stacked microstrip antenna fed by an L-probe for quadruple band operation", *IET Microwaves, Antennas & Propagation*, **9**, pp. 360-368 (2015). doi: 10.1049/iet-map.2014.0362

[19] Ali, A., Iqbal, A., Alibakhshikenari, M., et al. "Design process of a compact tri-band MIMO antenna with wideband characteristics for sub-6 GHz, Ku-band, and millimeter-wave applications", *Ain Shams Engineering Journal*, **15**(3), 102434 (2024). doi: 10.1016/j.asej.2023.102579

[20] Luo, Q., Pereira, J.R. and Salgado, H.M. "Compact printed monopole antenna with chip inductor for WLAN", *IEEE Antennas and Wireless Propagation Letters*, **10**, pp. 880-883 (2011). doi: 10.1109/LAWP.2011.2166049.

[21] Salonen, P., Keskilammi, M. and Kivikoski, M. "Single-feed dual-band planar inverted-F antenna with U-shaped slot", *IEEE Transactions on Antennas and Propagation*, **48**(8), pp. 1262-1264. doi: 10.1109/8.884498

[22] Pan, S. -C. and Wong, K. -L. "Dual-frequency triangular microstrip antenna with a shorting pin", *IEEE Transactions on Antennas and Propagation*, **45**(12), pp. 1889-1891 (1997). doi: 10.1109/8.650213

[23] Basaran, S.C. and Erdemli, Y.E. "A dual-band split-ring monopole antenna for WLAN applications", *Microwave and Optical Technology Letters*, **51**, pp. 2685-2688 (2009). doi: 10.1002/mop.24708

[24] Palandoken, M. "Dual broadband antenna with compact double ring radiators for IEEE 802.11 ac/b/g/n WLAN communication applications", *Turkish Journal of Electrical Engineering and Computer Sciences*, **25**(2), pp. 1198-1208 (2017). doi: 10.3906/elk-1507-121

[25] Yoon, J., Chul, R. and Lee, Y. "Design of a microstrip-fed monopole antenna with a rectangular slit ground and a rectangular projection strip for dual-band WLAN operations", *Microwave and Optical Technology Letters*, **54**(4), pp. 1022-1025 (2012). doi: 10.1002/mop.26725

[26] Lu, J. -H., Tang, C. -L. and Wong, K. -L. "Novel dual-frequency and broad-band designs of slot-loaded equilateral triangular microstrip antennas", *IEEE Transactions on Antennas and Propagation*, **48**(7), pp. 1048-1054 (2000). doi: 10.1109/8.876323

[27] Liu, S., Wu, W. and Fang, D. -G. "Single-Feed dual-layer dual-band E-shaped and U-slot patch antenna for wireless communication application", *IEEE Antennas and Wireless Propagation Letters*, **15**, pp. 468-471 (2016). doi: 10.1109/LAWP.2015.2453329

[28] Liu, S., Qi, S. -S., Wu, W., et al. "Single-Feed dual-band single/dual-beam U-slot antenna for wireless communication application", *IEEE Transactions on Antennas and Propagation*, **63**(8), pp. 3759-3764 (2015). doi: 10.1109/TAP.2015.2438331.

[29] Gao, S., Ge, L., Zhang, D. and Qin, W. "Low-Profile dual-band stacked microstrip monopolar patch antenna for WLAN and car-to-car communications", *IEEE Access*, **6**, pp. 69575-69581 (2018). doi: 10.1109/ACCESS.2018.2877420

[30] Radiall. "SMA adjustable square flange jack receptacle with cylindrical contact - R125414000", *Radiall Product Catalog*, https://www.radiall.com/sma-adjustable-square-flange-jack-receptacle-with-cylindrical-contact-r125414000.html

[31] Zhang, A., Wei, K., Hu, Y., et al. "High-Isolated coupling-grounded patch antenna pair with shared radiator for the application of 5G mobile terminals", *IEEE Transactions on Antennas and Propagation*, **70**(9), pp. 7896-7904 (2022). doi: 10.1109/TAP.2022.3168276

[32] Tran, H.H., Nguyen, T.T. and Nguyen, T.T. "Two closely spaced microstrip patches with high isolation for full-duplex/MIMO applications", *PLoS One*, **18**(10), e0290980 (2023). doi: 10.1371/journal.pone.0290980

Biographies

Yavuz Asci was born in Yalvaç, Turkey, in 1983. He received the B.Sc., M.Sc., and Ph.D. degrees from the Department of Electrical and Electronics Engineering at Dokuz Eylül University and Ege University, İzmir, Turkey, in 2008, 2014, and 2021, respectively. Since 2026, he has been an Associate Professor in the Department of Electrical and Electronics Engineering at Uşak University, Uşak, Turkey. His research interests include microstrip and waveguide satellite antennas, microwave/millimeter-wave front-ends, waveguide components, and 3D printing.

Kaan Bakircioglu is a PhD student in the Department of Electrical and Electronics Engineering at Yaşar University, İzmir, Turkey. He received the BSc and MSc degrees in Electrical and Electronics Engineering from Yaşar University in 2017 and 2020, respectively. He has been working toward the PhD degree in Electrical and Electronics Engineering at Yaşar University since 2020. His thesis focuses on EEG-based biometric identification and wireless EEG sensing systems. His research interests include EEG signal processing, biometric identification, neural networks, wireless communication, and embedded systems.

Mustafa Secmen was born in ˙Izmir, Turkey, in 1980. He received the B.S. and Ph.D. degrees from the Department of Electrical and Electronics Engineering, Middle East Technical University, Ankara, Turkey, in 2002 and 2008, respectively. He has been a Professor with Yasar University, Izmir since 2010. His current research interests include radar signal processing, the design and implementation of waveguide and microstrip antennas for satellite and wireless communication.

List of figure captions

Figure 1. Configuration of the proposed dual-band, single-feed antenna with structural parameters. (a) Top, (b) *YoZ* cut, (c) Side view
Figure 2. The surface current distributions at (a) 2.45 GHz and (b) 5.4 GHz.
Figure 3. Simulated reflection coefficients as a function of (a) outer patch length (*y2*), (b) transition width (*x8*), (c) grounded pin position (*y10*); Boresight gains as a function of (d) outer patch length (*y2*), (e) transition width (*x8*), (f) grounded pin position (*y10*). Units are in mm.
Figure 4. Simulated reflection coefficients as a function of (a) excitation pin position (*y7*), (b) *y6*, (c) outer patch width (*x1*); Boresight gains as a function of (d) excitation pin position (*y7*), (e) *y6*, (f) outer patch width (*x1*). Units are in mm.
Figure 5. Simulated reflection coefficients as a function of (a) stub length (*y8*), (b) inner patch width (*x12*), (c) inner patch length (*y4*); Boresight gains as a function of (d) stub length (*y8*), (e) inner patch width (*x12*), (f) inner patch length (*y4*). Units are in mm
Figure 6. Simulated reflection coefficients with and without parasitic patches: (a) lower and (b) upper frequency bands.
Figure 7. Fabricated dual-band antenna, (a) Radiation part (top view), (b) Grounded pin and SMA connector (side view).
Figure 8. (a) Measurement setup photo of $|S_{11}|$ for the proposed antenna (b) Screenshot of the measured $|S_{11}|$ in Anritsu MS2028C VNA (c) Radiation pattern measurement setup (in the anechoic chamber).
Figure 9. Simulation and measurement results of the proposed antenna (a) Reflection coefficients ($|S_{11}|$) and (b) Boresight gains.
Figure 10. Simulated and measured radiation patterns (a) E-plane at 2.45 GHz (b) H-plane at 2.45 GHz (c) E-plane at 5.4 GHz (d) H-plane at 5.4 GHz.

List of Table captions

Table 1. The ultimate dimensions for single-feed dual-band WLAN patch antenna (Unit: mm)
Table 2. Comparison of State-of the-Art Dual-Band WLAN Antennas

Figures:

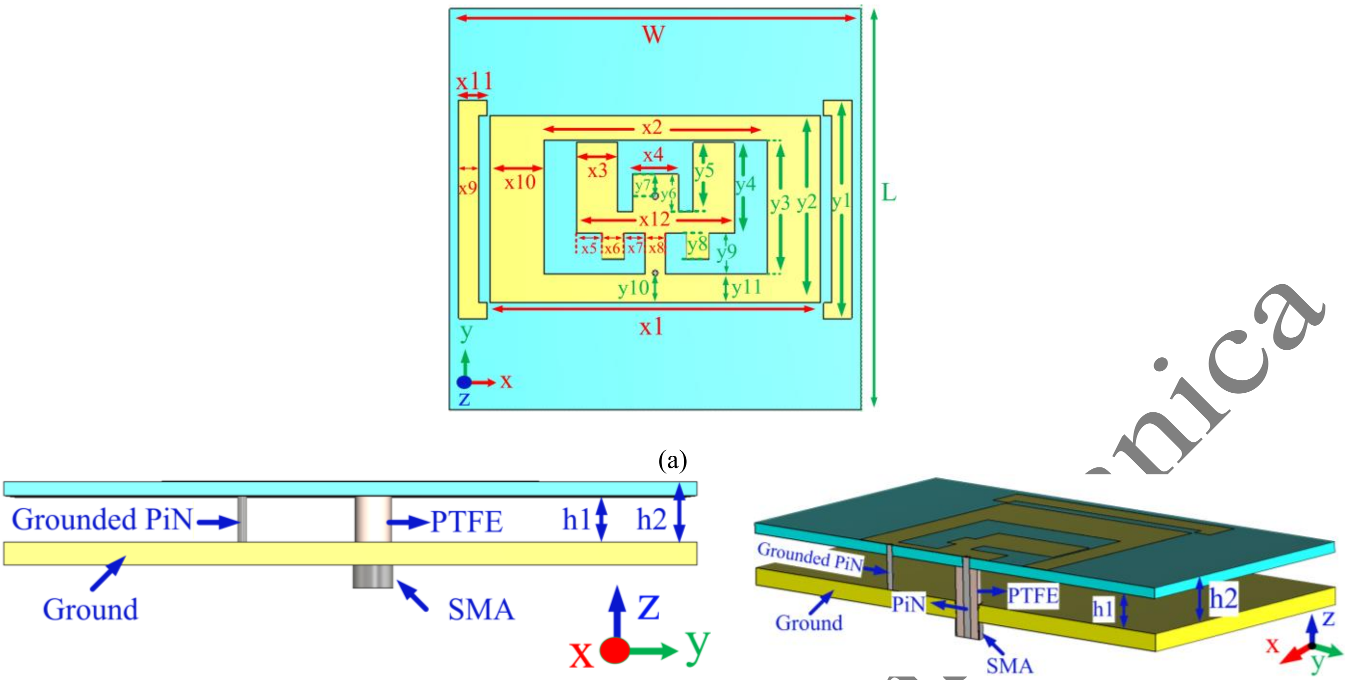

Figure 1. Configuration of the proposed dual-band, single-feed antenna with structural parameters. (a) Top, (b) *YoZ* cut, (c) Side view

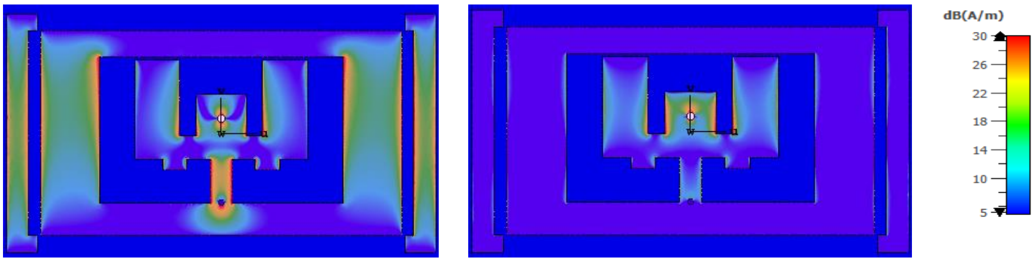

(a) (b)

Figure 2. The surface current distributions at (a) 2.45 GHz and (b) 5.4 GHz.

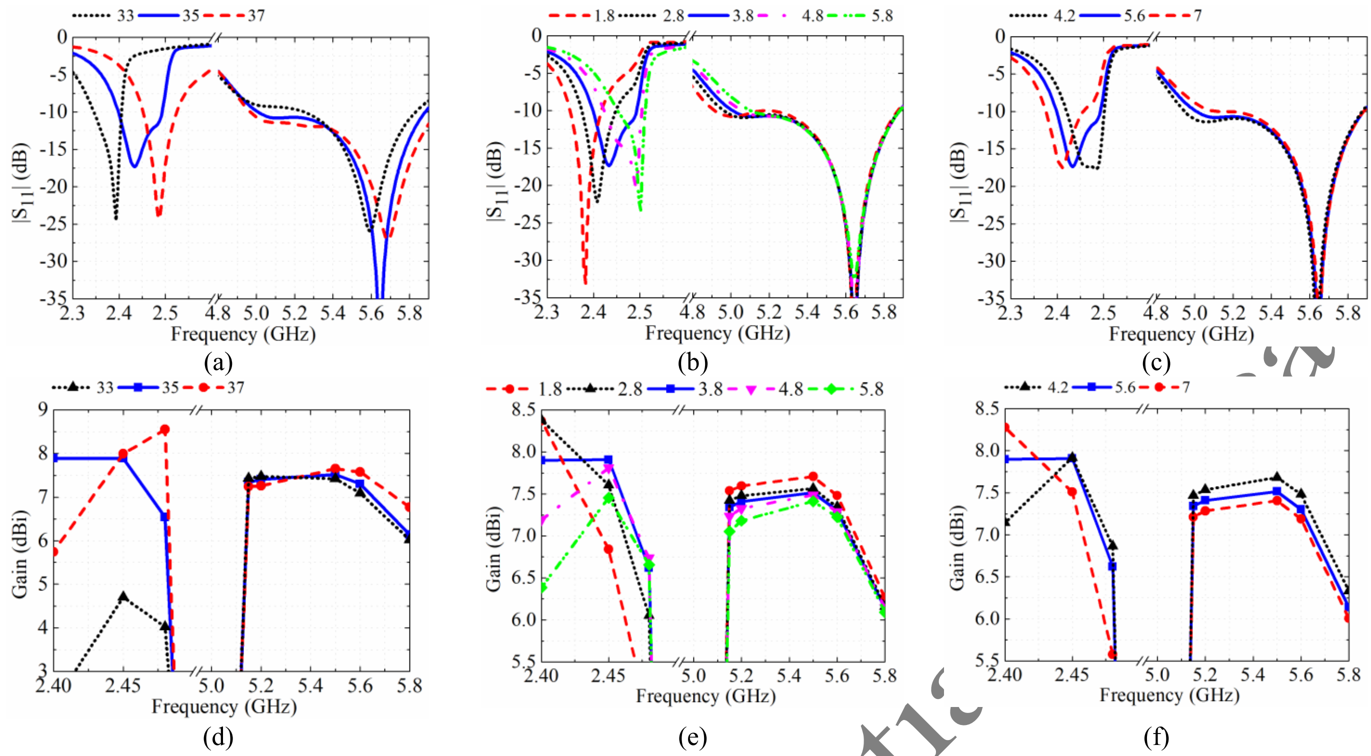

Figure 3. Simulated reflection coefficients as a function of (a) outer patch length (*y2*), (b) transition width (*x8*), (c) grounded pin position (*y10*); Boresight gains as a function of (d) outer patch length (*y2*), (e) transition width (*x8*), (f) grounded pin position (*y10*). Units are in mm.

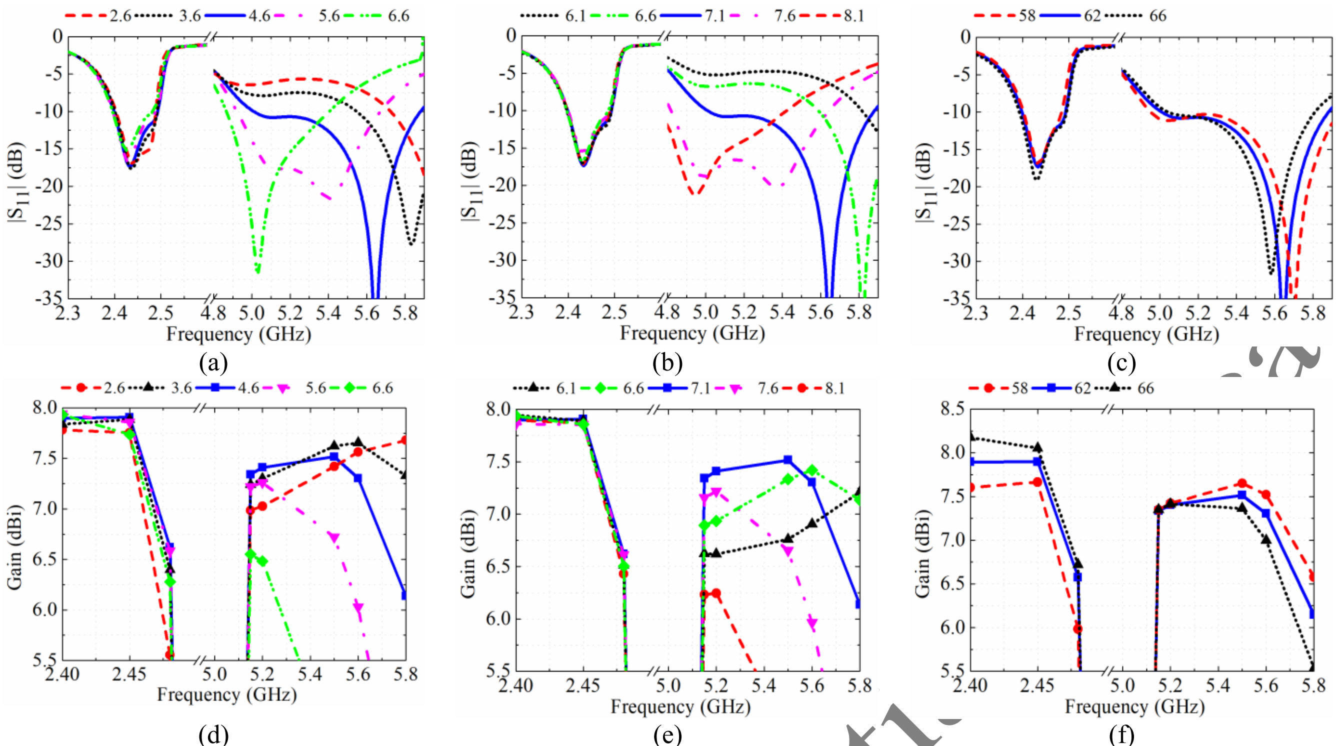

Figure 4. Simulated reflection coefficients as a function of (a) excitation pin position (*y7*), (b) *y6*, (c) outer patch width (*x1*); Boresight gains as a function of (d) excitation pin position (*y7*), (e) *y6*, (f) outer patch width (*x1*). Units are in mm.

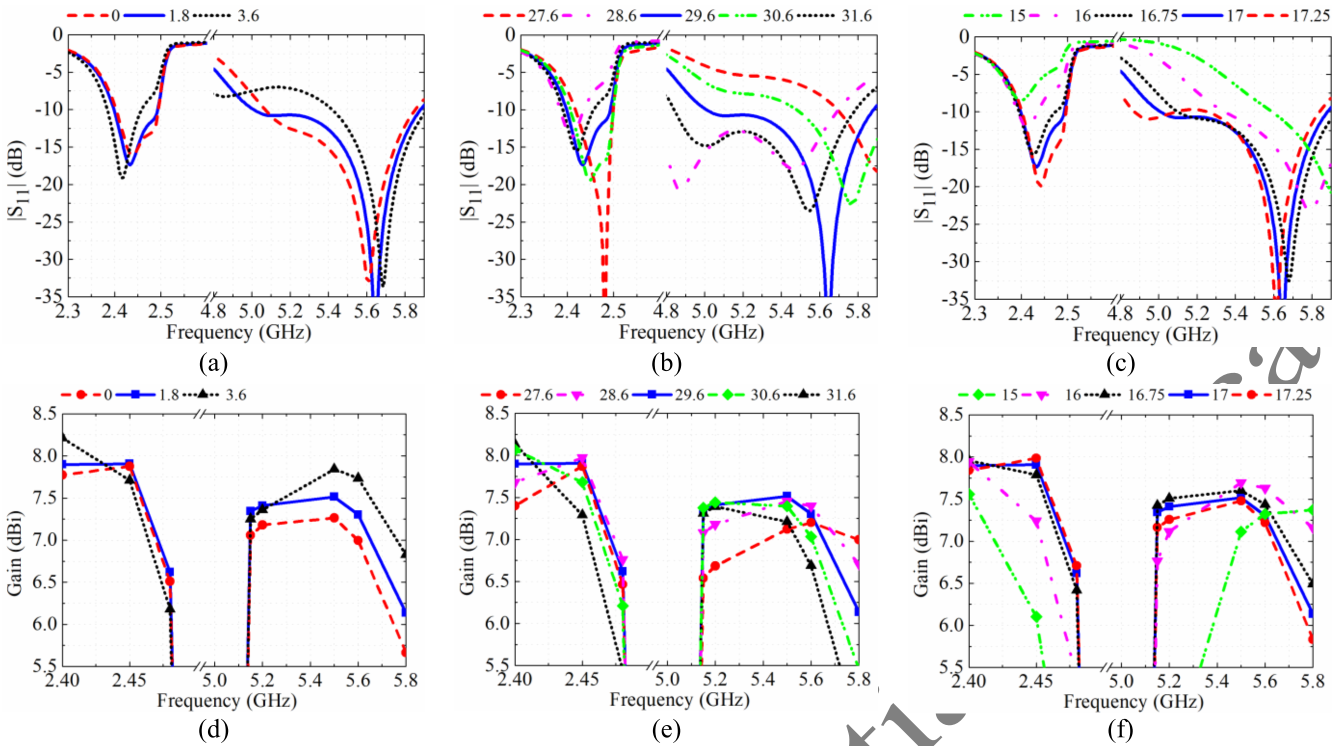

Figure 5. Simulated reflection coefficients as a function of (a) stub length (*y8*), (b) inner patch width (*x12*), (c) inner patch length (*y4*); Boresight gains as a function of(d) stub length (*y8*), (e) inner patch width (*x12*), (f) inner patch length (*y4*). Units are in mm.

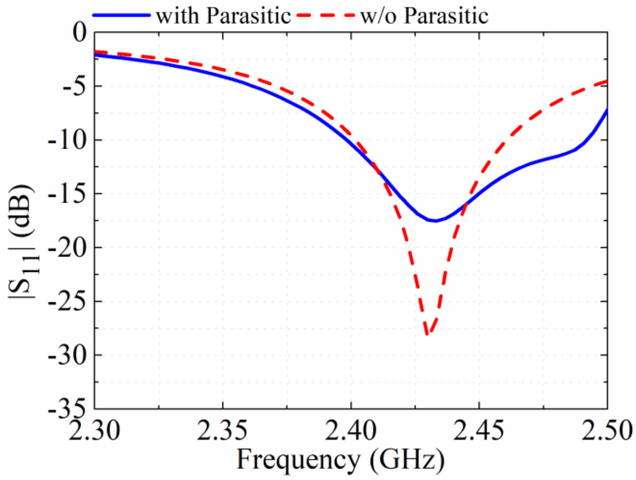

(a)

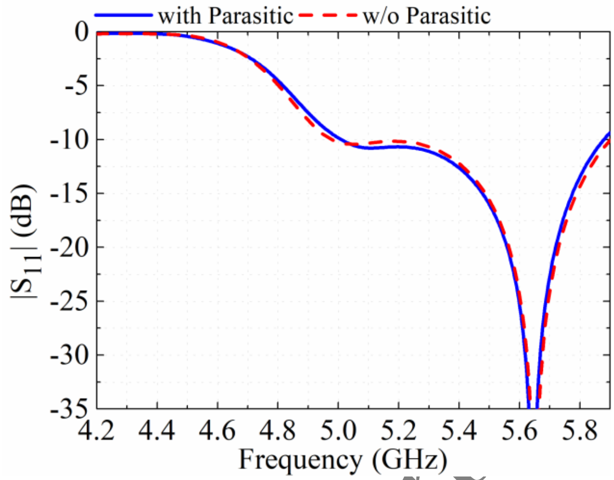

(b)

Figure 6. Simulated reflection coefficients with and without parasitic patches: (a) lower and (b) upper frequency bands.

(a) (b)

Figure 7. Fabricated dual-band antenna, (a) Radiation part (top view), (b) Grounded pin and SMA connector (side view).

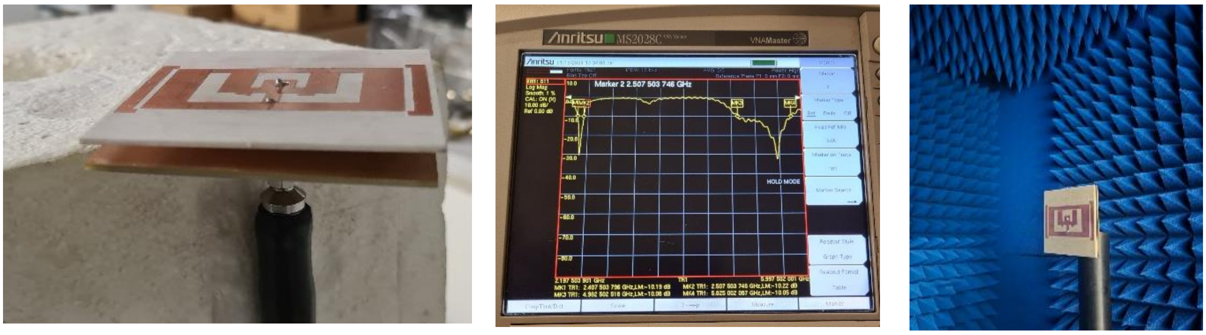

(a) (b) (c)

Figure 8. (a) Measurement setup photo of $|S_{11}|$ for the proposed antenna (b) Screenshot of the measured $|S_{11}|$ in Anritsu MS2028C VNA (c) Radiation pattern measurement setup (in the anechoic chamber)

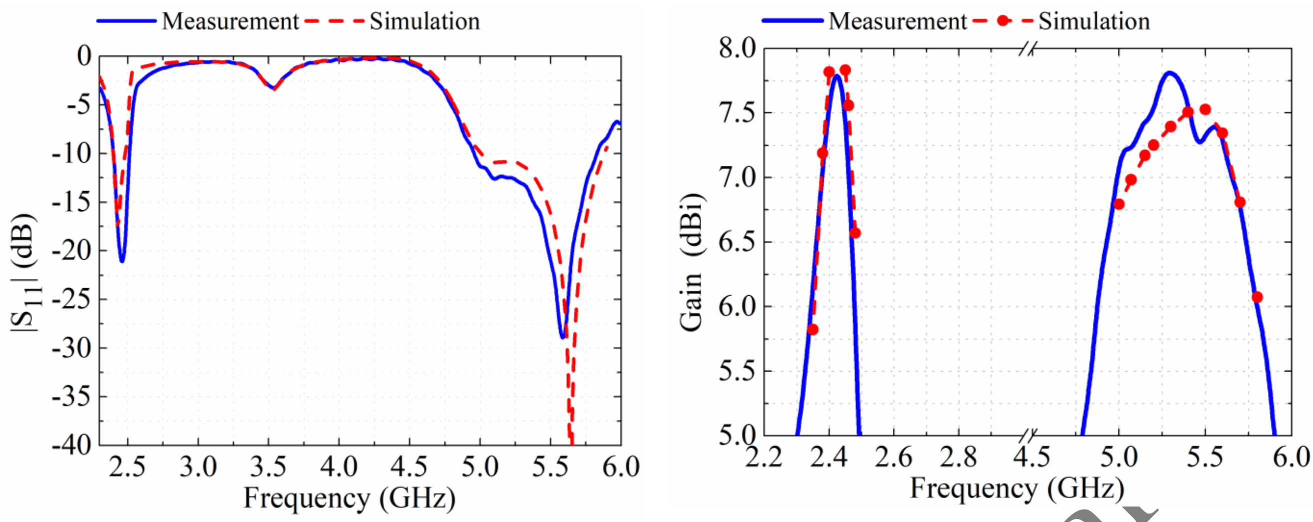

(a) (b)

Figure 9. Simulation and measurement results of the proposed antenna (a) Reflection coefficients ($|S_{11}|$) and (b) Boresight gains.

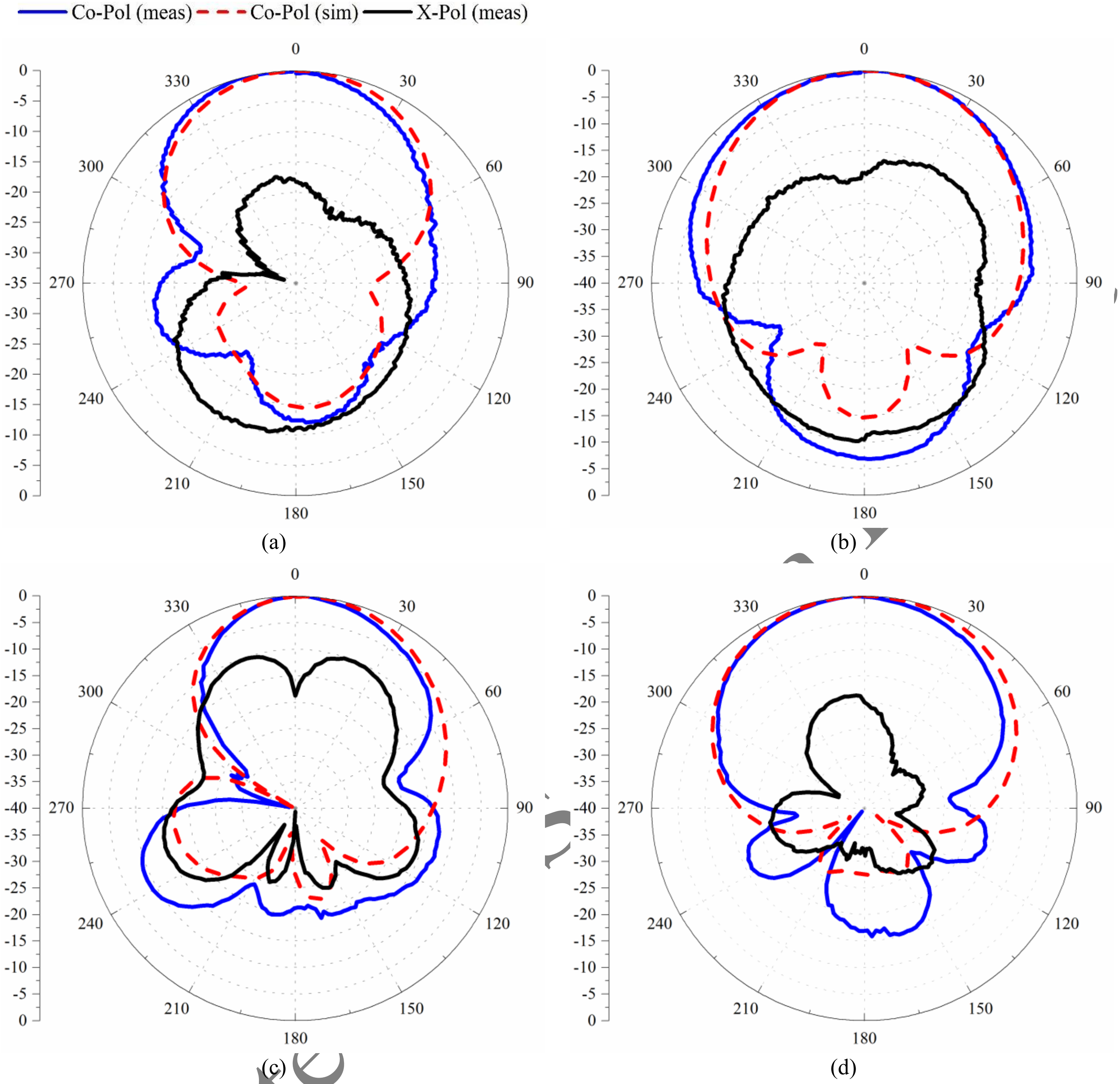

Figure 10. Simulated and measured radiation patterns (a) E-plane at 2.45 GHz (b) H-plane at 2.45 GHz (c) E-plane at 5.4 GHz (d) H-plane at 5.4 GHz.

Tables

Table 1. The ultimate dimensions for single-feed dual-band WLAN patch antenna (Unit: mm)

x1	***x2***	***x3***	***x4***	***x5***	***x6***	***x7***	***x8***	***x9***	***x10***	***x11***	***x12***	***W***	***L***
62	42.8	7.7	8.6	4.85	4.1	3.95	3.8	3.8	10.1	5.3	29.6	77	75
y1	***y2***	***y3***	***y4***	***y5***	***y6***	***y7***	***y8***	***y9***	***y10***	***y11***	***h1***	***h2***	
40.8	35	25	17	13	7.1	4.6	1.8	7.5	5.6	5.5	5	6.5	

Table 2. Comparison of State-of the-Art Dual-Band WLAN Antennas

Study	Frequency (GHz)		Peak Gain (dBi)		Volume (λ_c^3)
	Low Band	High Band	Low Band	High Band	W × L × H
[3]	2.37 – 2.63	5.52 – 6.37	5.2	6	1.20 × 1.20× 0.02
[10]	3.75 – 4.05	5.0 – 5.75	7.2	7.2	0.92 × 0.68 × 0.08
[20]	2.41 – 2.49	5.2 – 5.6	1.5	1.8	0.20 × 0.08 × 0.01
[24]	2.32 – 3.00	4.7 – 6	4.8	2.9	0.53 × 0.80 × 0.01
[25]	2.33 – 2.48	5.08 – 6.4	4.6	2.7	0.39 × 0.14 × 0.01
[27]	2.25 – 2.95	3.38 – 3.62	7.1	7.4	0.81 × 0.81 × 0.10
[28]	2.31 – 2.49	4.92 – 5.58	6.3	7.7	0.53 × 0.35 × 0.08
[29]	2.24 – 2.53	5.42 – 5.98	6	7.5	0.68 × 0.68 × 0.03
T.S.	2.39 – 2.51	4.95 – 5.82	7.8	7.5	0.62 × 0.61 × 0.05

N.A.: Not available; T.S.: This Study; All antennas bandwidth for $|S_{11}| < -10$ dB; λ_c = free-space wavelength at the center operating frequency of the lower band